Available online at www.sciencedirect.com
ScienceDirect
International Journal of Mass Spectrometry 260 (2007) 107–114
International Journal of Mass Spectrometry
www.elsevier.com/locate/ijms

NanoSIMS and EPMA analysis of nickel localisation in leaves of the hyperaccumulator plant *Alyssum lesbiacum*

K.E. Smart [a,*], M.R. Kilburn [a], C.J. Salter [a], J.A.C. Smith [b], C.R.M. Grovenor [a]

[a] *Department of Materials, University of Oxford, Parks Road, Oxford OX1 3PH, UK*
[b] *Department of Plant Sciences, University of Oxford, South Parks Road, Oxford OX1 3RB, UK*

Received 30 May 2006; received in revised form 21 August 2006; accepted 21 August 2006
Available online 12 September 2006

Abstract

Certain plants known as 'metal hyperaccumulators' can accumulate exceptional concentrations of elements such as zinc, manganese, nickel, cobalt, copper, selenium, cadmium or arsenic in their above ground tissue. In members of the genus *Alyssum*, nickel concentrations can reach values as high as 3% of leaf dry biomass. These plants must possess very effective mechanisms for the transport, chelation and sequestration of such elements within their tissues to avoid the toxic effects of free metal ions. Evidence from a number of different techniques suggests that nickel is concentrated primarily in the outermost, epidermal tissue of leaves of *Alyssum* hyperaccumulators, but there is currently no consensus on the principal sites of nickel sequestration. In this study, high resolution secondary ion mass spectrometry (NanoSIMS) analysis has been performed on longitudinal sections of *Alyssum lesbiacum* leaves. Elemental maps were obtained which revealed the high concentrations of nickel in the peripheral regions of the large unicellular stellate leaf hairs (trichomes) and in the epidermal cell layer. Electron probe microanalysis (EPMA) was used to provide independent confirmation of elemental distribution in the specimens, but the superior spatial resolution and high chemical sensitivity of the NanoSIMS technique provided a more detailed image of elemental distribution in these biological specimens at the cellular level.
© 2006 Elsevier B.V. All rights reserved.

Keywords: Hyperaccumulator plants; *Alyssum lesbiacum*; Nickel; Secondary ion mass spectrometry (NanoSIMS); Electron probe microanalysis (EPMA)

1. Introduction

Certain terrestrial plants can accumulate very high concentrations of potentially toxic metallic elements in their leaves and stems without suffering from any impairment of growth. Over 400 species of these so-called "metal hyperaccumulator" plants are now known [1,2]. These species tend to be restricted in their natural distribution to metalliferous soils, and they typically contain metal concentrations in their above ground tissues about two orders of magnitude higher than the great majority of plant species [3,4]. The threshold values for metal hyperaccumulattion have been defined as 1% of dry shoot biomass for zinc and manganese, 0.1% for nickel, cobalt, copper and selenium, and 0.01% for cadmium and arsenic although values as high as 5 and 3% of dry biomass have been recorded for zinc and nickel, respectively [1,2]. Due to the high degree of metal tolerance shown by hyperaccumulator plants, it is possible that they might find application in various forms of bioremediation treatment for the decontamination of metal-polluted soils [5–8].

To avoid the toxic effects of free metal ions, hyperaccumulator plants must possess effective mechanisms for the transport, chelation and sequestration of such elements within their tissues. Many of the membrane proteins responsible for metal transport throughout the plant have now been identified [9–11], as have some of the principal ligands involved in metal binding in different phases of the cell [3,9,12,13]. For example, uptake of nickel by hyperaccumulator plants is associated with a specific and proportional synthesis of the aminocarboxylic acid histidine, which strongly coordinates the incoming nickel and facilitates its translocation through the plant [14,15]. However, there is less certainty about the ultimate sites of metal sequestration within the shoots of hyperaccumulator plants. Consequently, there is a need for the application of novel techniques to help determine the sites of metal deposition in biological tissues at high resolution.

Within the shoot tissues of hyperaccumulator plants, metals may be stored in several distinct cellular compartments. Quantitatively the largest compartment is the central vacuole, which

* Corresponding author.
E-mail address: katharine.smart@st-annes.ox.ac.uk (K.E. Smart).

1387-3806/$ – see front matter © 2006 Elsevier B.V. All rights reserved.
doi:10.1016/j.ijms.2006.08.011

may occupy as much as 90% of cell volume in mature cells. In terrestrial plants, the cell vacuole typically contains high concentrations of hydroxycarboxylic acids (e.g., malic, citric, isocitric, malonic, tartaric acids); these can bind metal ions with moderately high affinity, but are thought unlikely to be responsible for the chemical specificity of metal hyperaccumulation [3,12,14]. Most enzymes of central metabolism are localised in the cell cytoplasm, and functional groups on proteins must be protected from inactivation by metal ions. This is achieved by appropriate high-affinity ligands (including low-molecular-weight metabolites, peptides and proteins), which buffer the cytoplasmic pool of transition metals and maintain the concentration of free metal ions at very low values. Finally, significant metal binding may also occur in the extracellular matrix of the cellulosic cell wall, in which considerable quantities of metal ions can be bound by the polygalacturonic acid residues of non-esterified pectins, and by wall-localised proteins.

Considerable work has been performed on nickel-hyperaccumulator plants to try to determine the principal sites of metal localisation within the shoots, but a consistent picture of nickel distribution within these tissues has not yet emerged. Using subcellular fractionation techniques, Krämer et al. [16] reported that 67–73% of the nickel in the leaves of *Thlaspi goesingense* is associated with the cell wall. In contrast, Küpper et al. [17] investigated metal localisation by a direct method involving energy dispersive X-ray (EDX) analysis of rapidly frozen hydrated material performed on a scanning electron microscope (SEM) with a cryostage attachment. These authors reported nickel to be localised predominantly in the vacuoles rather than the cell wall of leaves of *Alyssum bertolonii*, *Alyssum lesbiacum* and *T. goesingense*. Furthermore, Küpper et al. [17] found that for the three hyperaccumulator plants they studied, all showed preferential accumulation of nickel in the vacuoles of the outermost, epidermal cell layer of leaves; in contrast the mesophyll cells forming the ground tissue and cells in the central vascular tissue contained much less nickel, a pattern of metal accumulation that may be interpreted as protecting photosynthetic activity in the chloroplasts-containing mesophyll cells. Apart from differences in methodology, these contrasting results might also be a function of the precise conditions under which the plants were cultivated and the developmental age of the tissues examined.

Another distinctive structural feature of nickel-hyperaccumulator plants in the genus *Alyssum* is the presence of large, unicellular stellate hairs (trichomes) in the epidermis, which can form a sufficiently dense covering to give the shoot surface a silvery-whitish appearance, see Fig. 1. The EDX analyses of Küpper et al. [17] apparently indicated exclusion of nickel from the bulk of the trichomes of *A. bertolonii* and *A. lesbiacum*. However, evidence was obtained by SEM/EDX for a locally high concentration of nickel in the basal part of the trichome, which was confirmed by staining with the nickel reagent dimethylglyoxime [17]. These results differ somewhat from those of Krämer et al. [18], who used proton-induced X-ray emission (PIXE) with a spatial resolution of approximately 1 μm to examine dehydrated and fixed leaf specimens of *A. lesbiacum* prepared by molecular distillation drying. The PIXE results indicated that

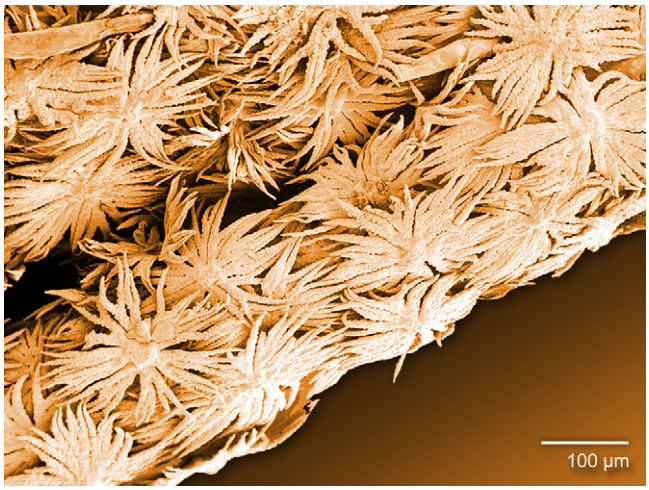

Fig. 1. Scanning electron micrograph of *A. lesbiacum* leaf surface showing the dense covering of stellate unicellular trichomes.

nickel is sequestered to a considerable degree in the epidermal trichomes, although this technique did not allow for the finer subcellular analysis needed to explore the mechanisms of sequestration. Again, the discrepancies in these reports concerning the sites of highest nickel concentration in leaves of *Alyssum* may be methodological. Dehydration and fixation prior to elemental mapping, as used by Krämer et al. [18], may lead to redistribution of mobile ions, even when the rate of sample dehydration is minimised. In localising nickel histochemically, Küpper et al. [17] immersed leaves in dimethylglyoxime for 3 h, then dissected and observed them optically. However, the trichomes of *Alyssum* are covered by a thick, waxy, hydrophobic cuticle, which may have hindered penetration of the dye; on detaching the trichomes from the leaf surface, the basal region was exposed to the dye but the thick waxy cuticle of the external surface remained intact, so the colorimetric reaction with nickel may have been favoured in the basal region of the trichomes.

There has also been a report by Psaras et al. [19], based on a study with SEM/EDX, that the epidermal trichomes of *Leptoplax emarginata* (a species closely related to *Alyssum*) do not accumulate nickel. These authors studied nickel accumulation in the leaf epidermis of dried herbarium material of eight hyperaccumulator species. In all species, nickel was apparently excluded from the trichomes and specialised stomatal guard cells. In some species, nickel was present at low levels in the subsidiary cells adjacent to the stomatal guard cells, while the sites of higher nickel accumulation were observed in epidermal cells away from the stomatal complex. Psaras et al. [19] suggested that these results indicate that nickel is not compatible with the specialised functions of cells in the stomatal complex, and concluded that nickel is sequestered mainly in the highly vacuolate and metabolically less active cells of the epidermis. However, the apparent absence of nickel from the trichomes reported by Psaras et al. [19] is in direct contradiction to both the PIXE results of Krämer et al. [18] and the colorimetric results of Küpper et al. [17]. In contrast, in the nickel hyperaccumulator *Thlaspi montanum* var. *siskiyouense* – a species that lacks epidermal trichomes – it has also been observed by SEM/EDX that nickel is present in sub-

sidiary cells of the stomatal complex, but is apparently absent from both the stomatal guard cells and the unspecialised epidermal cells [20].

In 2004, Broadhurst et al. [21] reported the co-localisation of high levels of nickel, manganese and calcium in certain regions of the trichomes of several species of *Alyssum* using SEM/EDX analysis. It was reported that nickel is stored either in *Alyssum* leaf epidermal cell vacuoles or in the basal portion only of the stellate trichomes, with no appreciable nickel detectable in the arms (rays) or surface features (nodules). However, calcium was strongly concentrated in the trichome rays and nodules [21,22]. More recently, McNear et al. [23] have used synchrotron-based fluorescence and absorption-edge computed microtomography to investigate speciation of nickel in leaves of *Alyssum*, although this technique lacks the spatial resolution required to map intracellular details of metal localisation at the subcellular level. The authors suggest that nickel is concentrated mainly in the vascular tissue, epidermal trichomes and basal compartments of trichomes, and is absent from the photosynthetically active mesophyll cells. Colocalisation of nickel with cobalt, zinc and manganese was observed in some specimens, suggesting that sites of metal deposition may be partly determined by pathways of delivery of metals to the shoot from the root in the transpiration stream [21,23,24].

To date, therefore, there is no complete consensus on the principal sites of nickel storage in the shoots of hyperaccumulator plants. New high resolution analytical methods would be valuable for obtaining independent evidence on sites of metal sequestration in plant tissues, especially at the sub-cellular level. Dynamic secondary ion mass spectrometry (SIMS) microscopy may provide such a method, although it has not yet been applied extensively to biological materials. It has been known for some 20 years that this technique may offer significant advantages for particular kinds of analysis, including exceptionally high sensitivities and high chemical specificity. Research in the life sciences using SIMS analysis began in 1982 with the work of Burns et al. [25], and 10 years later the whole of vol. 74 in the journal *Biology of the Cell* was dedicated to SIMS analysis of biological materials. When combined with the submicrometer lateral resolution of the latest generation of SIMS instrumentation, this technique can provide insight into many areas of biological research in which intracellular chemical variations in three dimensions are likely to be of critical importance.

The application of SIMS analysis to biological materials has been tested in a broad spectrum of studies; e.g., cancer research [26,27] and the study of nucleotidic base analogues used in antiviral or anticancer therapy [28,29]. In a SIMS study of soybean leaf *Glycine max*, Grignon et al. [30] showed that the easily diffusible, mobile ions potassium, calcium and magnesium in leaf tissue may be redistributed during chemical fixation and adsorbed onto certain cellular organelles. Recently, Hallegot et al. [31] reported results on the analysis of hair samples using high resolution SIMS, illustrating how the distribution of trace elements can be determined in organic samples.

In the present study, we have investigated the application of high resolution SIMS to the localisation of nickel in tissues of the hyperaccumulator plant *A. lesbiacum*, to determine whether the combination of analytical sensitivity and high spatial resolution (sub-150 nm) offered by this technique can provide new insight into nickel localisation at the cellular and subcellular levels in these tissues.

2. Materials and methods

2.1. Sample preparation

The samples used in this investigation were taken from the previous MicroPIXE study of Krämer et al. [18], in which full details of sample preparation are given. Briefly, plants of the nickel hyperaccumulator *A. lesbiacum* (Candargy) Rech.f. (Brassicaceae) were grown from seed collected from an ultramafic (serpentine) soil on Lesbos, Greece. After germination, plants were cultivated on a 1:1 mixture of perlite and nickel-containing serpentine topsoil from the Lizard Peninsula, Cornwall, UK.

To minimise the extent of mobile-ion redistribution during specimen preparation, samples of leaf tissue were frozen in liquid propane immediately after excision from the plant. The frozen tissue was then slowly dehydrated over 5 days under vacuum ($<10^{-4}$ Pa) by molecular distillation drying at the triple point of water. The heating rate was $1\,^{\circ}C\,h^{-1}$ from a temperature of -190 to $-70\,^{\circ}C$, which was increased to a rate of $10\,^{\circ}C\,h^{-1}$ from -70 to $+20\,^{\circ}C$. Once at room temperature, specimens were vapour fixed with paraformaldehyde and embedded in L.R. White resin.

Sections from the embedded specimens were cut on an ultramicrotome to a thickness of 8–10 μm. These were transferred in a droplet of water to a support film made of Pioloform resin (Agar Scientific Ltd.). The water was then evaporated by gentle heating thereby adhering the sections to the film. Samples could be stored permanently in this state without significant deterioration. For analysis by NanoSIMS, the sectioned material was excised from the support film, floated onto 7 mm × 7 mm silicon squares, and gently warmed to allow good adherence to the silicon surface.

Samples were examined by confocal light microscopy and SEM to identify cell types in the leaf cross-section. The micrograph in Fig. 2 shows a typical sample after analysis in the NanoSIMS. The darker square is the area rastered by the incident ion beam, and the darker spots in the resin layer between the two leaf surfaces may be a result of local beam damage. Similar damage in the leaf section itself is not observed, hence it is believed that elemental distributions in the *A. lesbiacum* sample are not significantly perturbed by beam damage.

2.2. Analytical methods

Electron probe microanalysis (EPMA) of biological materials has been established for over 30 years [32]. In this work, EPMA was performed using a JEOL 8800R with an accelerating voltage of 20 kV and a beam current of 20 nA. The Kα lines of Ca, K, Mg and Ni were measured simultaneously on four wavelength-dispersive spectrometers to minimise beam damage

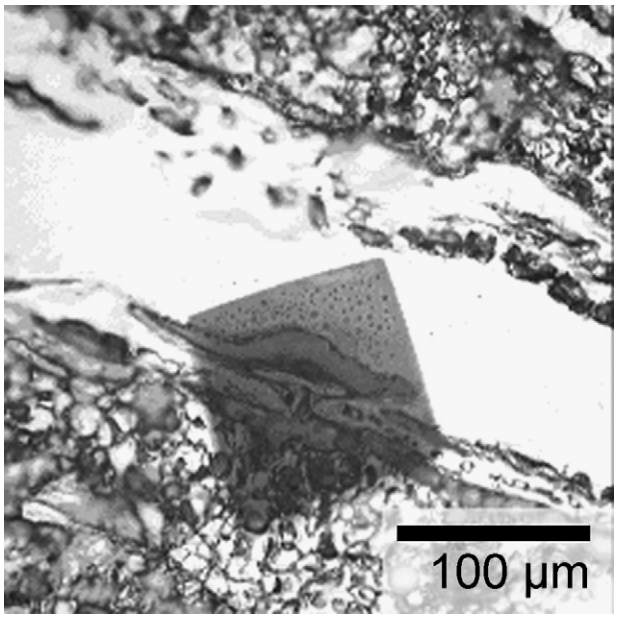

Fig. 2. Light micrograph of longitudinal leaf sections of *A. lesbiacum* showing the upper section of one leaf and the lower section of second leaf. A cross-section of one of the trichomes analysed is visible inside the square feature created by beam damage in the NanoSIMS raster.

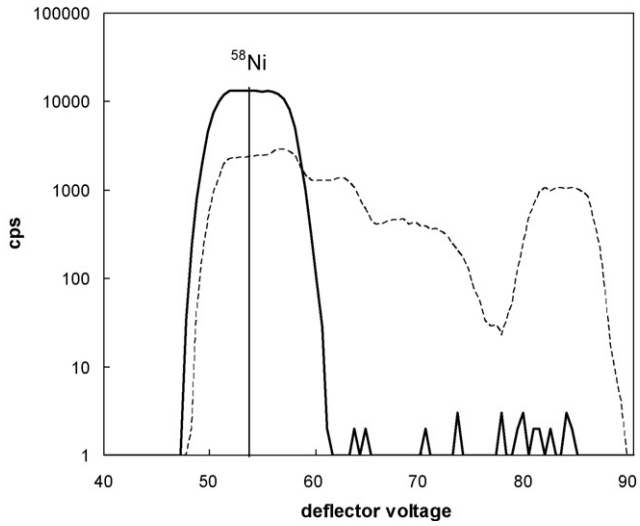

Fig. 3. Overlaid high resolution mass spectra around 58 a.m.u. from nickel standard (bold line) and plant specimen (dashed line). The higher mass peaks in the plant spectrum are tentatively identified as being from ions like $^{29}Si_2$, ^{40}Ca, ^{16}O, $^{1}H_2$ and $^{14}N_4$, $^{1}H_2$.

to the sample. Apatite, orthoclase, magnesium oxide and nickel metal were used as standards for Ca, K, Mg and Ni, respectively. ZAF matrix corrections [33] were used for quantitative elemental analysis assuming a matrix of cellulose. Detection limits were typically between 50 and 100 ppm for these elements in this organic matrix.

The CAMECA NanoSIMS 50 is a new generation of dynamic SIMS that allows simultaneous collection of five ion species with high mass and high spatial resolution. A primary ion beam is scanned across the surface of the sample, and the sputtered secondary ions are extracted to a double focusing mass spectrometer. The NanoSIMS is capable of sub-50 nm lateral resolution whilst imaging negatively charged secondary ions (with Cs^+ primary ions) and sub-150 nm lateral resolution for positive secondary ions (with O^- primary ions) [34].

In this experiment negative secondary ions were sputtered using a Cs^+ primary beam, with a beam current of 4 pA, rastered over an area approximately 100 μm × 100 μm. Ion maps of $^{12}C^-$, $^{16}O^-$, $^{12}C^{14}N^-$, $^{32}S^-$, $^{58}Ni^-$ and $^{60}Ni^-$, together with

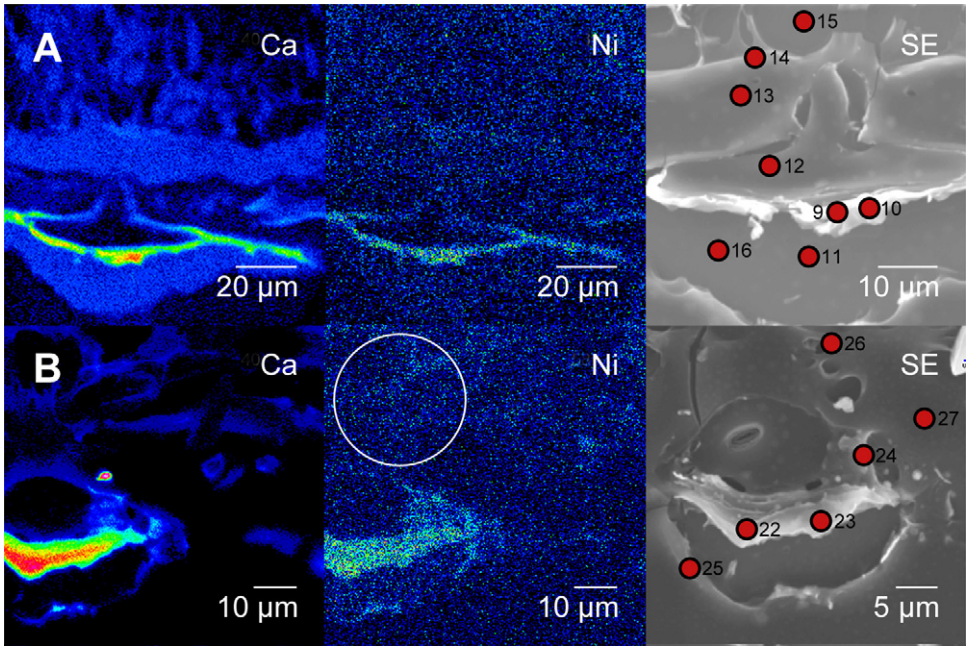

Fig. 4. EPMA elemental maps for Ca, Ni and (slightly magnified) secondary electron (SE) images of the central region of three trichomes A and B.

secondary electron images were produced at a resolution of approximately 250 nm. Although the primary beam was focused to a smaller diameter, the resolution was determined by the pixel size (256 × 256) in order that longer count times could be used to enhance the sensitivity. Positive secondary ions, $^{23}Na^+$, $^{40}Ca^+$, $^{58}Ni^+$ and $^{60}Ni^+$ were sputtered using an O^- primary beam, with a beam current of 25 pA, rastered over the same area. The resolution of images obtained using the O^- primary beam is constrained by the diameter of the beam to 300–400 nm. The instrument was tuned for high mass resolution in order to exclude isobaric interferences. A nickel metal standard was used to calibrate the secondary ion signal, and the two isotopes ^{58}Ni and ^{60}Ni were imaged to confirm the peak selection. Fig. 3 is a high resolution mass spectrum around mass 58 a.m.u. and presents an overlay of the spectrum from the nickel metal standard and the *A. lesbiacum* sample. The ^{58}Ni peak from the nickel standard is precisely aligned with the first of several overlapping peaks from the plant sample. Taking account the significant mass deficit for nickel (∼−80 milli-mass units), the detector tuning for ^{58}Ni can be positioned at the setting indicated by the vertical line in the figure with confidence.

In all cases, the area was implanted and cleaned with the primary ion beam prior to analysis. After analysis, the depth of the etch pits was measured and found to be several tens of nanometres, indicating that surface contamination was removed before the images were acquired.

3. Results

Both EPMA and NanoSIMS analysis were carried out on longitudinal sections of leaves of the nickel-hyperaccumulator plant *A. lesbiacum* prepared by molecular distillation drying, focusing particularly on the distinctive epidermal trichomes. These sections, previously studied by MicroPIXE [18], give directly comparable images of the 2-D distribution of sequestered nickel.

Table 1
Electron microprobe microanalysis (EPMA) of elemental composition of trichome and epidermal tissues of *A. lesbiacum*

Point	Ni (%, w/w)	K (%, w/w)	Ca (%, w/w)	Mg (%, w/w)
9	0.57 ± 0.17	1.84 ± 0.55	3.90 ± 1.17	0.39 ± 0.12
10	1.15 ± 0.35	1.08 ± 0.32	8.33 ± 2.50	0.37 ± 0.11
11	n.d.[a]	1.28 ± 0.38	1.29 ± 0.39	0.55 ± 0.17
12	n.d.	0.77 ± 0.23	0.43 ± 0.13	0.16 ± 0.05
13	n.d.	1.13 ± 0.34	0.50 ± 0.15	0.22 ± 0.07
14	n.d.	0.65 ± 0.20	0.38 ± 0.11	0.16 ± 0.05
15	n.d.	2.11 ± 0.63	1.08 ± 0.32	0.57 ± 0.17
16	n.d.	2.30 ± 0.69	1.26 ± 0.38	0.59 ± 0.18
22	1.07 ± 0.32	2.41 ± 0.72	10.77 ± 3.23	1.08 ± 0.33
23	0.86 ± 0.26	2.93 ± 0.88	9.30 ± 2.79	0.75 ± 0.23
24	0.15 ± 0.05	0.43 ± 0.13	0.95 ± 0.28	0.17 ± 0.05
25	n.d.	0.19 ± 0.06	0.22 ± 0.07	0.02 ± 0.01
26	0.05 ± 0.02	0.18 ± 0.05	0.58 ± 0.17	0.04 ± 0.01

The numbered points refer to the regions identified in Fig. 3; values are expressed as elemental content as a percentage of section mass and are given as means ± S.D. ($n = 2$ samples).

[a] n.d. indicates not detectable (i.e., value below the detection limit).

3.1. EPMA analysis

EPMA X-ray maps of calcium, nickel and secondary electron (SE) images are shown for three different epidermal trichomes in Fig. 4. All three trichomes show enrichment of Ca and Ni in the cell wall on the outer surfaces of the trichome. EPMA allows quantitative analyses to be readily undertaken, and Table 1 shows the concentrations of nickel, calcium and potassium determined for several points in and around the central portion of the trichomes, as illustrated in Fig. 4.

These data show that the background concentration of nickel in many parts of the specimen is below the detection limit of the electron microprobe technique, i.e., less than 100 ppm (Table 1).

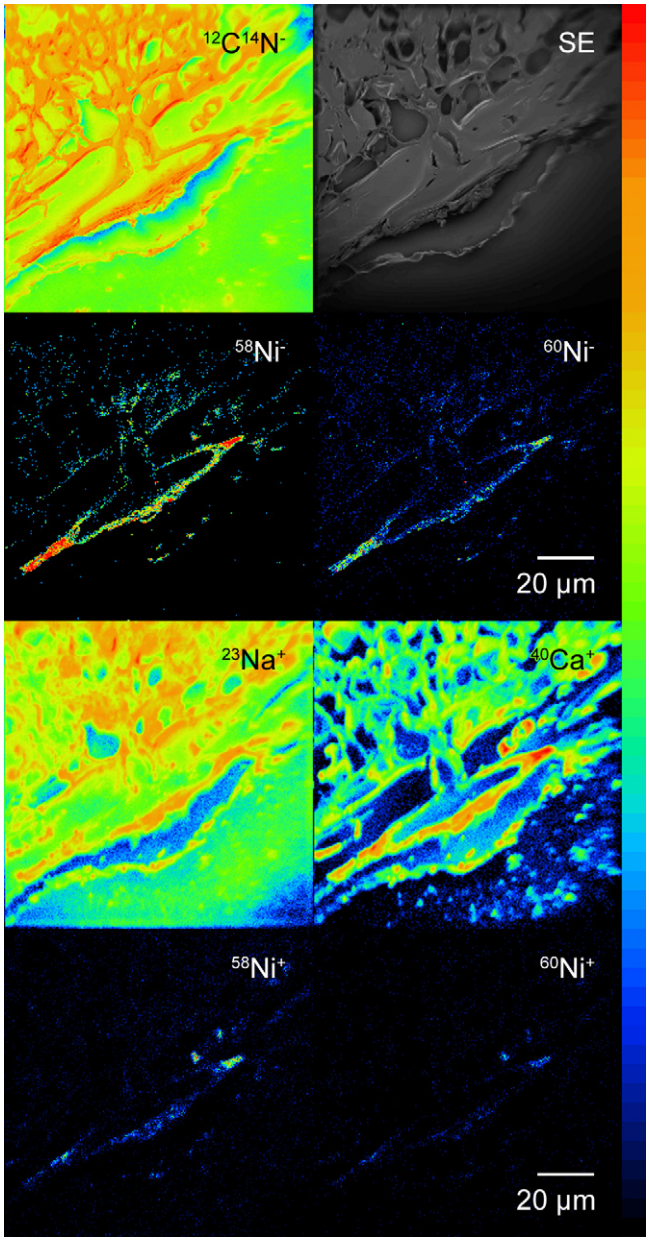

Fig. 5. NanoSIMS elemental maps of trichome A showing elemental maps obtained using both beam polarities: Cs^+ to map $^{12}C^{14}N^-$, SE, $^{58}Ni^-$ and $^{60}Ni^-$ (upper four panels), and O^- to map $^{23}Na^+$, $^{40}Ca^+$, $^{58}Ni^+$ and $^{60}Ni^+$ (lower four panels).

In specific regions of the trichome, however, the localised concentration of nickel can exceed 1% (w/w), reaching a maximum of 1.15% (w/w). These calculations are based on ZAF matrix corrections that assume a matrix composed of 99% cellulose, which potentially can give rise to errors of up to ±30%. Even taking this possible error into account, it is clear that the cell walls of the trichome can be enriched in nickel to concentrations of the order of 1% (w/w). Calcium is present throughout the tissue, but is strongly enriched in the trichome – up to 10.8% (w/w) – and the concentrations of nickel and calcium in the wall phase are reasonably closely correlated (Table 1). Krämer et al. [18] reported concentrations of 0.62% (w/w) nickel and 7.7% (w/w) calcium in these epidermal trichomes using PIXE, which is in good agreement with the EPMA data presented here. The concentrations of potassium and magnesium, i.e., 1.0% (w/w) and 0.35% (w/w), respectively were more constant throughout the tissue, but were also comparable to the values of Krämer et al. [18].

3.2. NanoSIMS analysis

NanoSIMS analysis was undertaken of the same specimens prior to the EPMA analysis because of the serious damage that the incident electron beam creates in the sample surface. Fig. 5 shows negative and positive secondary ion elemental maps of the cross-section of trichome A, obtained using the Cs^+ and O^- beams, respectively. The SE image shows the structure and integrity of the sample surface. The $^{12}C^{14}N^-$ ion image is typically used to illustrate morphology in organic materials [35], and here reveals the cell wall outline and some intracellular structure. The large stellate trichome is clearly visible in radial cross-section, with its stalk embedded in the outermost (epidermal) cell layer of the leaf. The $^{58}Ni^-$ ion image shows nickel enrichment in the radial edges and outermost walls of the trichome. Transverse sections of trichome rays are also visible in the $^{12}C^{14}N^-$ image as the two rounded features with high nickel content between the epidermal cell layer and the central trichome ray. The regions of significant nickel enrichment extend into the lowest basal part of the trichome stalk, situated between the epidermal cell layer and underlying ground tissue (mesophyll cells). This may reflect the pathway by which nickel is transported through the leaf and delivered to the basal part of the epidermal trichome.

Images obtained using a positive beam polarity are also presented in Fig. 5, but with poorer spatial resolution due to the larger incident beam size. The $^{23}Na^+$ image reveals the structural integrity of the surface, and is comparable to a secondary electron image. Sodium has a very high positive ion yield, and even low, naturally occurring concentrations in organic materials produce bright images. As with the SE image, charging effects due to topography or holes in the surface are more evident in the $^{23}Na^+$ map. Although some dark regions (indicating holes) are present between some of the cells, the images generally appear flat with no significant artefacts due to charging. The $^{40}Ca^+$ map shows the outline of cellular structure, much like the $^{12}C^{14}N^-$ image, but reveals enrichment of this element in the cell walls of the trichome. As with the negative secondary ion images, the $^{58}Ni^+$ map displays a strong enrichment of Ni in the cell wall of the trichome. As expected, the $^{60}Ni^+$ signal mirrors the $^{58}Ni^+$ signal, but at lower intensity proportional to its isotopic abundance, providing a useful control for possible mass interference in the elemental signals.

The data presented in Fig. 6 shows for one further trichome (B) that Ca and Ni are both present at their highest concentrations in the cell wall phase of these structures, particularly in the trichomes and epidermal cells. It is clear that the spa-

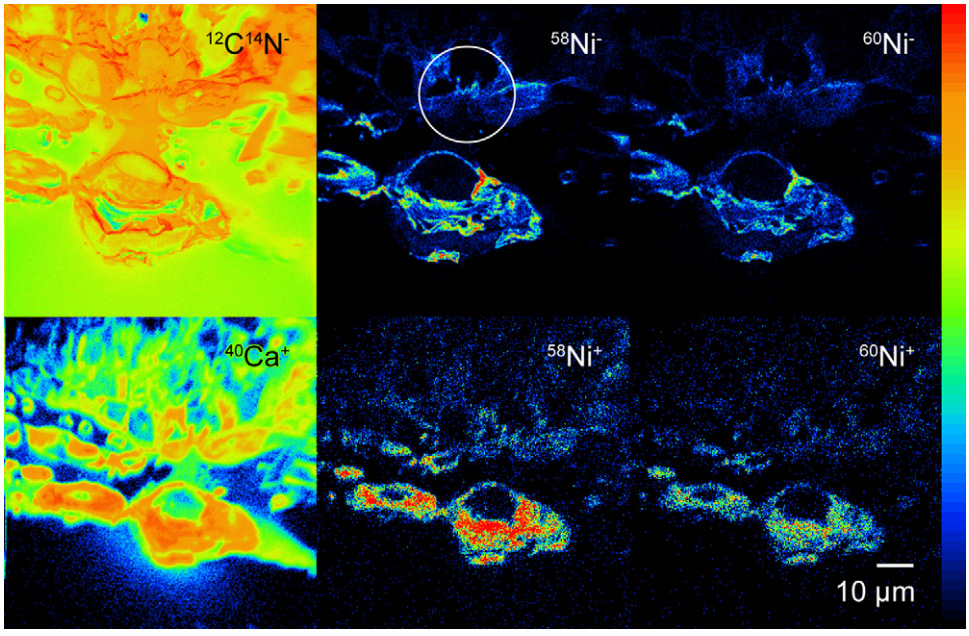

Fig. 6. NanoSIMS elemental maps of trichome B showing elemental maps obtained using both beam polarities: Cs^+ to map $^{12}C^{14}N^-$, $^{58}Ni^-$ and $^{60}Ni^-$ (upper three panels), and O^- to map $^{40}Ca^+$, $^{58}Ni^+$ and $^{60}Ni^+$ (lower three panels).

tial resolution is better in the $^{58}Ni^-$ image than in the $^{58}Ni^+$ image due to the smaller incident beams size. The higher sensitivity of the NanoSIMS also allows the metal distribution in the epidermal cells to be more clearly revealed than in the EPMA images of the same trichome in Fig. 4. (see circled areas in Figs. 4 and 6).

Comparing the EPMA nickel maps in Fig. 4 and the nickel ion maps in Figs. 5 and 6 it can be seen that from identical trichomes the two analytical techniques give similar distributions of sequestered metal. We are thus confident that these chemical maps are a reliable indication of the distribution of nickel in these *A. lesbiacum* specimens.

4. Discussion and conclusions

This study demonstrates that NanoSIMS is a powerful technique for identifying sites of metal localisation in plant tissues. The technique has sufficient spatial resolution and analytical sensitivity to allow the distribution of elements in such specimens to be mapped at the cellular level. Nevertheless, the technique is susceptible to a number of potential practical limitations when applied to biological specimens. For example, contrast in chemical images in a SIMS instrument can be produced in a variety of ways; including by topography, differential matrix yields, as well as by real variations in species concentration. Plant material has strong local matrix density variation, so it is not expected that ion yield across a specimen surface will be uniform. However, the variation in the nickel concentrations suggested by the NanoSIMS chemical maps presented here are not a result of differential yield or topographical effects because the $^{12}C^{14}N^-$ and $^{58}Ni^-$ and, $^{40}Ca^+$ and $^{58}Ni^+$ maps in Figs. 4–6 are significantly different. In addition, the combination of EPMA and NanoSIMS in this study provides independent confirmation of the patterns of elemental distribution in the specimens. Another concern with biological material is the method used to dehydrate the specimens prior to analysis. The molecular distillation technique applied here is intended to minimise the redistribution of soluble elements as the specimen is dehydrated, because of the very slow rate of lyophilization [18]. However, the extent of possible elemental redistribution during sample preparation is an important factor in the preparation of biological specimens for NanoSIMS. A comparison of specimens dehydrated by lyophilization with those prepared by the method of freeze substitution (e.g., [36–38]) would be valuable to determine whether the two preparative methods give comparable results.

These results from both EPMA and NanoSIMS suggest that the epidermal trichomes represent a site of preferential nickel accumulation in the leaves of the hyperaccumulator plant *A. lesbiacum*. These findings are consistent with those of Krämer et al. [18], but are at variance with those of Broadhurst et al. [21], who detected nickel in the basal region of the trichomes but not in the rays. The NanoSIMS images also show some degree of nickel enrichment in the basal portion of the trichome, but to a much lesser degree than in the raised stellate region. Also of note is the observation of a significant epidermal cell accumulation of nickel, which concurs with the reports of Broadhurst et al. [21] and Küpper et al. [17] of high concentrations of nickel in leaf epidermal cell vacuoles.

Acknowledgements

This work was supported by funding from UK EPSRC grant GR/T19797/01 and the EU Research Training Network METALHOME (HPRN-CT-2002-00243).

References

[1] A.J.M. Baker, R.R. Brooks, Biorecovery 1 (1989) 81.
[2] R.D. Reeves, A.J.M. Baker, in: I. Raskin, B.D. Ensley (Eds.), Phytoremediation of Toxic Metals: Using Plants to Clean Up the Environment, John Wiley and Sons, New York, 2000, pp. 193–221.
[3] A.J. Pollard, K.D. Powell, F.A. Harper, J.A.C. Smith, Crit. Rev. Plant Sci. 21 (2002) 539.
[4] M.R. Macnair, Adv. Bot. Res. 40 (2003) 63.
[5] D.E. Salt, R.D. Smith, I. Raskin, Annu. Rev. Plant Physiol. Plant Mol. Biol. 49 (1998) 643.
[6] S.P. McGrath, F.J. Zhao, E. Lombi, Adv. Agron. 75 (2002) 1.
[7] E.A.H. Pilon-Smits, Annu. Rev. Plant Biol. 56 (2005) 15.
[8] U. Krämer, Curr. Opin. Biotechnol. 16 (2005) 133.
[9] S. Clemens, M.G. Palmgren, U. Krämer, Trends Plant Sci. 7 (2002) 309.
[10] J.L. Hall, L.E. Williams, J. Exp. Bot. 54 (2004) 2601.
[11] E.P. Colangelo, M.L. Guerinot, Curr. Opin. Plant Biol. 9 (2006) 322.
[12] N.P. Bhatia, K.B. Walsh, A.J.M. Baker, J. Exp. Bot. 56 (2005) 1343.
[13] D.L. Callahan, A.J.M. Baker, S.D. Kolev, A.G. Wedd, J. Biol. Inorg. Chem. 11 (2006) 2.
[14] U. Krämer, J.D. Cotter-Howells, J.M. Charnock, A.J.M. Baker, J.A.C. Smith, Nature 379 (1996) 635.
[15] R.A. Ingle, S.T. Mugford, J.D. Rees, M.M. Campbell, J.A.C. Smith, Plant Cell 17 (2005) 2089.
[16] U. Krämer, I.J. Pickering, R.C. Prince, I. Raskin, D.E. Salt, Plant Physiol. 122 (2000) 1343.
[17] H. Küpper, E. Lombi, F. Zhao, G. Wieshammer, S.P. McGrath, J. Exp. Bot. 52 (2001) 2291.
[18] U. Krämer, G.W. Grime, J.A.C. Smith, C.R. Hawes, A.J.M. Baker, Nucl. Instrum. Methods B 130 (1997) 346.
[19] G.K. Psaras, T.H. Constantinidis, B. Cotsopoulos, Y. Manetas, Ann. Bot. 86 (2000) 73.
[20] S.M. Heath, D. Southworth, J.A. D'Allura, Int. J. Plant Sci. 158 (1997) 184.
[21] C.L. Broadhurst, R.L. Chaney, J.S. Angle, T.K. Maugel, E.F. Erbe, C.A. Murphy, Environ. Sci. Technol. 38 (2004) 5797.
[22] C.L. Broadhurst, R.L. Chaney, J.S. Angle, E.F. Erbe, T.K. Maugel, Plant Soil 265 (2004) 225.
[23] D.H. McNear Jr., E. Peltier, J. Everhart, R.L. Chaney, S. Sutton, M. Newville, M. Rivers, D. Sparks, Environ. Sci. Technol. 39 (2005) 2210.
[24] D.H. McNear Jr., R. Tappero, D.L. Sparks, Elements 1 (2005) 211.
[25] M.S. Burns, J. Mic. 127 (1982) 237.
[26] S. Chandra, D. Lorey, Cell. Mol. Biol. 47 (2000) 503.
[27] S. Chandra, D.R. Lorey, D.R. Smith, Radiat. Res. 157 (2002) 700.
[28] J.L. Guerguin-Kern, Microsc. Res. Tech. 36 (1997) 287.
[29] P. Fragu, C. Briancon, C. Fourre, J. Clerc, O. Casiraghi, J. Jeusset, F. Omri, S. Halpern, Biol. Cell 74 (1992) 5.
[30] N. Grignon, S. Halpern, J. Jeusset, C. Briancon, P. Fragu, J. Microsc. 186 (1997) 51.
[31] P. Hallegot, R. Peteranderl, C. Lechene, J. Invest Dermatol. 122 (2004) 381.
[32] W.L. Robinson, in: C.A. Anderson (Ed.), Microprobe Analysis, John Wiley & Sons, New York, 1973, p. 271.
[33] D.B. Williams, J.I. Goldstein, C.E. Fiori, in: D.C. Joy, A.D. Romig Jr., J.I. Goldstein (Eds.), Principles of Analytical Electron Microscopy, Plenum Press, New York, 1986, p. 123.

[34] http://www.cameca.fr/doc_en_pdf/ns50_instrumentation_booklet_dec2002_150dpi_web.pdf, p. 5.
[35] N. Grignon, S. Halern, A. Gojon, P. Fragu, Biol. Cell 74 (1992) 143.
[36] S.D. Bidwell, S.A. Crawford, I.E. Woodrow, J. Sommer-Knudsen, A.T. Marshall, Plant Cell Environ. 27 (2004) 705.
[37] D. Budka, J. Mesjasz-Przybyłowicz, G. Tylko, W.J. Przybyłowicz, Nucl. Instrum. Methods B 231 (2005) 338.
[38] D.R. Fernando, G.N. Batianoff, A.J. Baker, I.E. Woodrow, Plant Cell Environ. 29 (2006) 1012.